Testing and Calibration Procedures for Mistuning Identification and Traveling Wave Excitation of Blisks

Darren E. Holland
e-mail: deholla@umich.edu

Matthew P. Castanier
e-mail: mpc@umich.edu

Steven L. Ceccio
e-mail: ceccio@umich.edu

Bogdan I. Epureanu
e-mail: epureanu@umich.edu

Department of Mechanical Engineering,
University of Michigan,
Ann Arbor, MI 48109

Sergio Filippi
Aeromechanics Technology,
GE Advanced Mechanical Design,
Cincinnati, OH 45245
e-mail: sergio.filippi@ge.com

In this work, an integrated testing and calibration procedure is presented for performing mistuning identification (ID) and traveling wave excitation (TWE) of one-piece bladed disks (blisks). The procedure yields accurate results while also being highly efficient and is comprised of three basic phases. First, selected modes from a tuned blisk finite element model are used to determine a minimal set of measurement degrees of freedom (and locations) that will work well for mistuning ID. Second, a testing procedure is presented that allows the mistuning to be identified from relatively few vibration response measurements. A numerical validation is used to investigate the convergence of the mistuning ID results to a prescribed mistuning pattern using the proposed approach and alternative testing strategies. Third, a method is derived to iteratively calibrate the excitation applied to each blade so that differences among the blade excitation magnitudes can be minimized for a single blade excitation, and also the excitation phases can be accurately set to achieve the desired traveling wave excitation. The calibration algorithm uses the principle of reciprocity and involves solving a least-squares problem to reduce the effects of measurement noise and uncertainty. Because the TWE calibration procedure re-uses the data collected during the mistuning ID, the overall procedure is integrated and efficient. [DOI: 10.1115/1.3204656]

1 Introduction

It is well known that small differences among blades, called mistuning, can lead to severe increases in the maximum vibration amplitude and stress levels of bladed disks [1–3]. The increased stress can cause premature high cycle fatigue failure [4]. Therefore, it is of interest to experimentally identify mistuning and assess the mistuned forced response characteristics of actual, manufactured bladed disks. Mistuning values are typically quantified by variations in the blade-alone natural frequencies. One can measure the natural frequencies of individual blades directly for disks with inserted blades, but not for one-piece bladed disks (blisks). Therefore, several techniques have been developed recently [5–24] to perform mistuning identification (ID) based on experimental measurements of the vibration response of a (full) blisk. While many of these studies have presented general mistuning ID experiments [5,6,9,25,11–13,16,20,22,23] methods for improving the efficiency and convergence of the testing procedure have not been considered. Another emerging area for mistuning testing is the use of traveling wave excitation (TWE) systems to mimic the engine-order-excitation patterns that blisks experience in an engine. For both TWE and mistuning ID, it is important to calibrate the excitation system. Normally, this calibration involves the measurement of the excitation output from each actuator [20]. However, performing the mistuning ID and calibrating the TWE system using existing methods require considerable time and effort.

In this work, an integrated testing and calibration procedure is presented for performing mistuning ID and TWE of blisks. The procedure yields accurate results while also being highly efficient and is comprised of three basic phases. First, selected modes from a tuned blisk finite element model (FEM) are used to determine a minimal set of measurement degrees of freedom (DOFs) (and locations) that will work well for mistuning ID. Second, a testing procedure is presented that allows the mistuning to be identified from relatively few vibration response measurements. A numerical validation is used to investigate the convergence of the mistuning ID results to a prescribed mistuning pattern using the proposed approach and alternative testing strategies. Third, a method is derived to iteratively calibrate the excitation applied to each blade so that differences among the blade excitation magnitudes can be minimized for a single blade excitation, and also the excitation phases can be accurately set to achieve the desired traveling wave excitation. The calibration algorithm uses the principle of reciprocity and involves solving a least-squares problem to reduce the effects of measurement noise and uncertainty. Because the TWE calibration procedure re-uses the data collected during the mistuning ID, the overall procedure is integrated and efficient.

2 Mistuning Model

The mistuning ID method used for this paper is based on the component mode mistuning proposed by Lim et al. [19], where the mistuned portion of the blisk is projected onto tuned cantilevered blade modes. Also, differences in the tuned system eigenvalues are identified. These differences are due to discrepancies between the finite element model and the actual blisk. More details are provided in the work of Madden et al. [24].

The mistuning ID requires the use of a FEM to determine the mode shapes of the tuned blisk and of its cantilevered blades. This paper uses a FEM of a "validation blisk" developed by Judge [25] and shown in Fig. 1. This 24 bladed blisk is cyclically symmetric (with very low manufacturing mistuning) and offers the ability to accurately apply known mistuning (with desired patterns).

Figure 2 displays the tuned natural frequencies and the corresponding nodal diameters calculated using ANSYS for the tuned FEM. Since the mistuning ID assumes that measurements are taken in the blade dominated region, the candidate cantilevered

Contributed by the International Gas Turbine Institute of ASME for publication in the JOURNAL OF ENGINEERING FOR GAS TURBINES AND POWER. Manuscript received March 27, 2009; final manuscript received April 3, 2009; published online January 25, 2010. Review conducted by Dilip R. Ballal. Paper presented at the ASME Gas Turbine Technical Congress and Exposition, Orlando, FL, June 8–12, 2009.

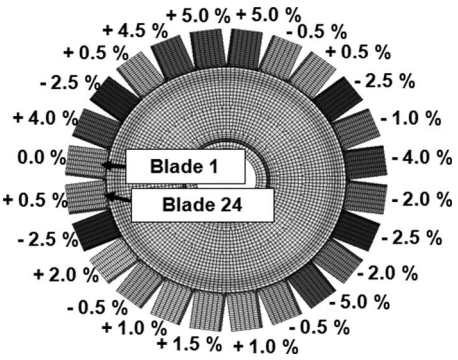

Fig. 1 Finite element model and mistuning values for the validation blisk

mode shapes and measured responses for the first flex (1F) modal family are between 1900 Hz and 2180 Hz, which excludes the disk dominated and veering frequencies of the 1F family.

Starting with the tuned model, one may add a random mistuning pattern (with values, for example, from −5% to +5% of the blade resonant frequencies). Figure 1 shows the mistuning pattern applied to the blades. Computing this pattern is the goal of the mistuning ID. The exact mode shapes and natural frequencies for the full mistuned model using the same mistuning pattern can also be computed using ANSYS. Blade 1 is arbitrarily chosen from the 24 blades, with the rest of the blade numbers increasing in a clockwise manner.

3 Test Procedure

The three main components of the experimental setup are the excitation system, the measurement equipment, and a supporting structure. The excitation consists of speakers, piezoelectric actuators, or magnets, which are placed on the opposite side of the measurement face of the blades. For traveling wave excitation and calibration, one excitation source (speaker, actuator, or magnet) is required behind each blade. A laser vibrometer is used to measure vibration velocities at locations (on the blade), which correspond to the nodes used in the finite element model. Lastly, the setup includes a vibration table with custom built supports for the blisk and excitation sources [25].

The measurement process includes three key issues, as examined in this section. First, the measured (locations and) DOFs on the blisk are chosen so that their motion can be used to accurately measure the response magnitude for the tuned modes in a chosen frequency range. Next, the order in which the blades are to be excited is chosen. Mistuning ID requires the excitation of only one blade at a time, referred to as a single blade excitation. The final component of the test procedure is choosing the excitation (and measurement) frequencies so that the mistuning ID is accurate and requires as few measurements as possible. Sections 3.1–3.3 discuss each of these issues.

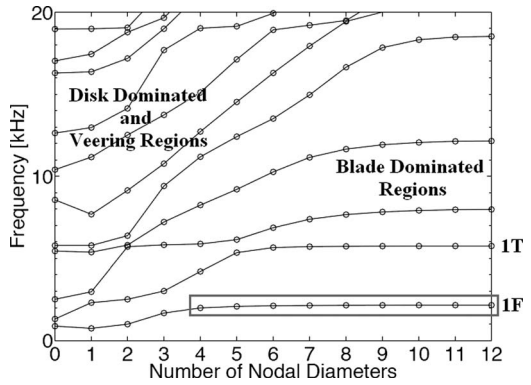

Fig. 2 Nodal diameters versus natural frequencies for the tuned validation blisk

3.1 DOF Selection. Before measurement data may be collected and the mistuning ID completed, the measurement DOF (and locations) on the blisk must be established. The measured DOF determine how the actual blisk motion, and mode shapes are captured by the measurements. For mistuning ID, the modes to be captured are tuned system modes. When the blisk motion is well represented by the measurement DOF, the mistuning ID error is less and the solution converges faster, requiring less measurements and laboratory time.

The approach to establish measurement points (and DOF) is the effective independence distribution vector (EIDV) method [26]. The EIDV method starts with the selection of a large set of candidate measurement DOF. Next, the EIDV method eliminates 1 DOF at a time until a much smaller set of DOF is selected. The algorithm ensures that this smaller set of DOF provides the most linearly independent measurements for the desired modes. In general, the set of candidate DOF should contain the largest number of DOF, which can be physically measured. DOFs that are typically not considered as candidate DOFs include points on the edge of the blade or on an irregular surface such as the disk-blade interface, where the measurement is not reliable. For the validation blisk, the candidate DOFs are all displacements normal to the surface of the blade, above the disk-blade interface, which are not along the blade edges (see Fig. 5).

In general, the modes of interest are related to expected potential forced vibration problems in an operating environment. However, the modes that have to be measured (for mistuning ID) are a subset of these modes of interest. The subset of modes is selected within the mistuning ID procedure/algorithm. While this subset of modes of interest is chosen automatically during the mistuning ID (with the rest being ignored), no method is currently available to determine which modes will comprise the subset *prior* to the actual mistuning ID. Therefore, the EIDV method must use all the modes of interest. As such, the EIDV procedure is based on a larger set of modes than is actually (strictly) needed for the mistuning ID. This approach allows the construction of a model that has much fewer DOF than the original parent FEM, and yet is very accurate for the mistuning ID [20,24]. The reduced order model (ROM) is based on tuned system modes.

Next, a brief overview of the EIDV procedure is discussed, closely following Penny et al. [26]. An EIDV matrix **E** is defined as

$$\mathbf{G} = \mathbf{U}_{\text{cand}}^{\text{ROM}^T}\mathbf{U}_{\text{cand}}^{\text{ROM}} \tag{1}$$

$$\mathbf{E} = \mathbf{U}_{\text{cand}}^{\text{ROM}}\mathbf{G}^{-1}\mathbf{U}_{\text{cand}}^{\text{ROM}^T} \tag{2}$$

where **G** is the Fisher information matrix and $\mathbf{U}_{\text{cand}}^{\text{ROM}}$ is the reduced modal matrix [27]. This reduced modal matrix is a portion of the full modal matrix for the blisk. Specifically, the columns of $\mathbf{U}_{\text{cand}}^{\text{ROM}}$ correspond to the tuned mode shapes to be measured. The rows correspond to the candidate DOF. The diagonal entries of **E** represent the fractional contribution of each measured DOF to the independence of the measurements for the given set of modes. The DOF with the lowest value on the diagonal of **E** is considered to contribute the least to the independence. Hence, this DOF is eliminated and the EIDV matrix is recalculated. Figure 3 shows schematically the process whereby EIDV reduces the number of measurement DOF, where N_{ROM} is the number of tuned system modes selected in the ROM, N_{all} is the number of all DOFs in the parent FEM of the full blisk, N_{cand} is the number of candidate measurement DOF for the full blisk, and N_{meas} is the final number of measurement DOF selected for the full blisk.

Note that the EIDV process is suboptimal because the initial

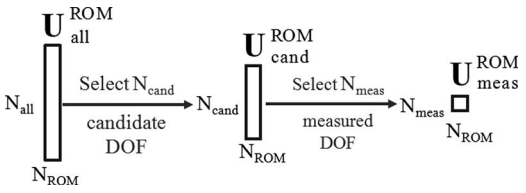

Fig. 3 Size of the system model matrix as DOFs are removed from consideration

selection of the candidate DOF is arbitrary and because it is assumed that the minimum entry on the diagonal EIDV matrix corresponds to the best point to remove at each iteration of the algorithm.

The overall set of candidate DOF contains measurement locations on all blades. However, on a blisk, the measurement points are the same on all blades. Thus, an assumption is made that the level of independence provided by the DOF on one blade is the same for each of the other blades. Therefore, instead of removing one DOF at a time, *n* DOFs are removed at a time (one on each blade), where *n* is the number of blades.

Table 1 summarizes EIDV results obtained using the unmodified EIDV method. Note that any given DOF on one blade is labeled the same on all blades. Hence, for example, DOF 1 refers to 1 DOF on a blade, and each blade has a DOF labeled as DOF 1. When 24 DOFs were retained, 23 of the DOFs were the same but on distinct blades. Only one blade retained a different DOF. When 48 DOFs were retained, 23 out of 24 blades had the same 47 DOFs, with only one blade having a different DOF. In addition, an examination of the diagonal entries of the EIDV matrix also supports removing the same DOF on all blades at the same time (as a set instead of individually).

For the mistuning ID, the EIDV procedure is applied until the reduced modal matrix $\mathbf{U}_{\text{cand}}^{\text{ROM}}$ would lose full rank if any other DOF (per blade) is removed. For example, if there are 24 blades and 17 modes in $\mathbf{U}_{\text{cand}}^{\text{ROM}}$, a minimum of 24 DOFs (1DOF per blade) is required. However, if there are 24 blades and 32 modes in $\mathbf{U}_{\text{cand}}^{\text{ROM}}$, a minimum of 48 DOFs (2DOF per blade) is required because the rank of $\mathbf{U}_{\text{cand}}^{\text{ROM}}$ must be at least 32. Figure 4 displays the algorithm implemented for the modified EIDV process.

Note that it is also possible to specify a larger number of DOF per blade to be measured than the minimum required by the loss of rank of the reduced modal matrix. Results of the EIDV procedure for six measured DOFs per blade, and a frequency range 0–5000 Hz are shown in Fig. 5. This frequency range includes both first flexural bending (1F) and first torsion (1T) modes of the validation blisk. The numbers in Fig. 5 indicate the ranking order of the DOF based on the EIDV values. For example, the DOF marked "1" is considered the best DOF to measure, "2" is the second-best, and so forth. For this case, a minimum of two points per blade are required. Note that these EIDV results make physical sense, because the two highest-ranked points are in locations that feature high response levels for both mode types (1F and 1T), but also feature different relative motions for each mode type.

3.2 Blade Selection. For the single blade excitation used in current mistuning ID approaches, a potential measurement frequency range is chosen, then a blade is excited at a resonant frequency in that range, and the mistuned response of the blade is

Table 1 DOF chosen using unmodified EIDV method; DOFs 1–3 refer to distinct measurement DOF on a blade

Total DOF retained	No. of DOF 1	No. of DOF 2	No. of DOF 3
24	23	1	
48	24	23	1

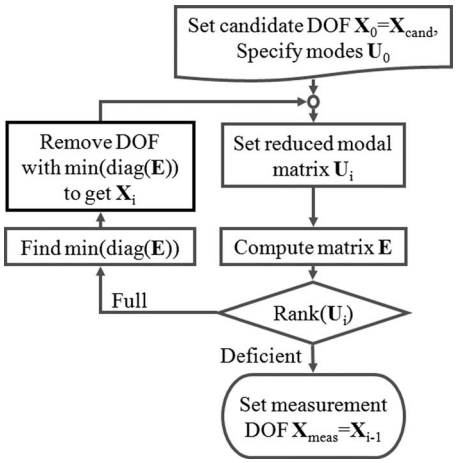

Fig. 4 Modified EIDV algorithm for mistuning ID

measured. In this section and in Sec. 3.3, an alternate test procedure is presented. There are two improvements to blade and frequency selection, which result in a new test procedure. This procedure is referred to as the maximum test procedure, and is shown to provide better results than the current sequential method test procedure. The sequential method involves excitations using sequential blade and frequency selection, and provides the basis for comparison.

The process for both methods starts by choosing an initial blade. This single blade is excited, and measurements are collected at all frequencies in a given range. Then, a neighboring blade is excited and responses are measured. The process repeats until all the desired measurements are completed or all frequencies in the frequency range of interest are measured for all blades. This blade selection pattern is used in the sequential test procedure. However, an alternate approach to excite the blisk that causes the mistuning ID to converge faster while producing better accuracy is advantageous. Since localization and structural damping tend to confine energy to the general area of the excited blade, the blade on the opposite side of the blisk typically has a low response magnitude for a blade dominated frequency. For a more disk dominated frequency, all the blades have similar response magnitudes. Hence, exciting multiple blades, one at a time, is desirable. After exciting one blade, choosing the next blade to excite to be on the opposite side of the blisk provides more complete and less redundant information about the system as compared with forcing another blade nearby the already excited blade.

To substantiate this claim, Fig. 6 shows two mistuned mode

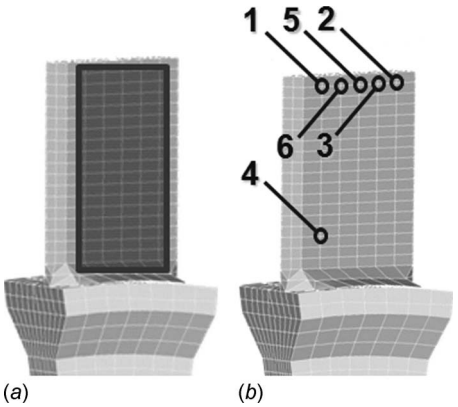

Fig. 5 Candidate DOFs are the displacements of the shaded region (left) and highest-ranked EIDV DOFs for the frequency range 0–5000 Hz (right)

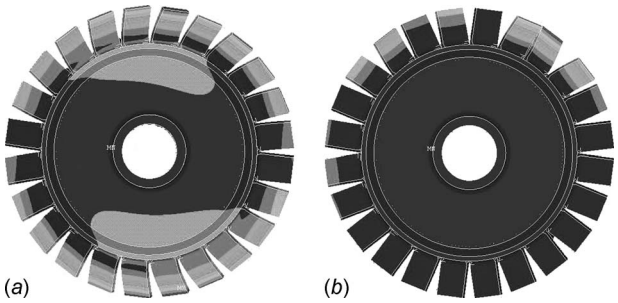

Fig. 6 Mode shapes for a blisk with 5% mistuning: almost tuned mode (left); mistuned mode (right)

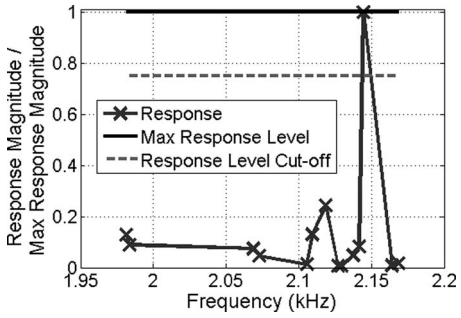

Fig. 8 Sample response results for the validation blisk excited at blade 9 for a 75% response level cut-off

shapes generated by ANSYS. The left figure shows the response of an approximately tuned blisk where any opposing blade pair has approximately the same response magnitude. In contrast, the right figure shows that localization results in a significantly decreased response on the opposite side of the blisk. Also, note that even if a tunedlike mode is to be measured, choosing the opposite blade generally does not result in less complete information than choosing a blade adjacent to the currently excited blade.

These observations result in what herein is referred to as the geometric blade selection pattern, shown in Fig. 7. The first blade to be excited is chosen arbitrarily. The pattern repeats by splitting the blisk into fourths, then eights, and so on. When switching between section types (e.g., halves to fourths), the first blade chosen is in the clockwise direction from the initial blade.

3.3 Frequency Selection. Two methods for choosing the measurement frequencies are presented in this section. The first method establishes excitation frequencies by first choosing the lowest frequency, and then selecting the next higher resonant frequency in the frequency range of interest for one blade. This method is used for the sequential test procedure. For instance, initially blade 9 might be excited at frequency 1994.5 Hz. Next, the second excitation is applied at blade 9 and 1995.0 Hz (the next higher resonant frequency for blade 9), followed by exciting the same blade at 2087.1 Hz (the next higher resonant frequency for blade 9), and so on. The responses of all DOFs determined using the EIDV method are collected at these frequencies. These measurements may then be used for the mistuning ID.

This method follows from the fact that, if all the blades are tested at all their resonant frequencies, the mistuned response will be fully explored. The reason the frequencies are selected from lowest to highest is to decrease the convergence time (for the mistuning ID) since strong localization only provides information on a few blades. However, weak localization results in little useful information about mistuning. If the frequency range includes many disk dominated modes, faster convergence may be achieved if the frequencies are selected from highest to lowest. If needed, the testing can continue until all blades have been excited at all their resonant frequencies in the frequency range of interest.

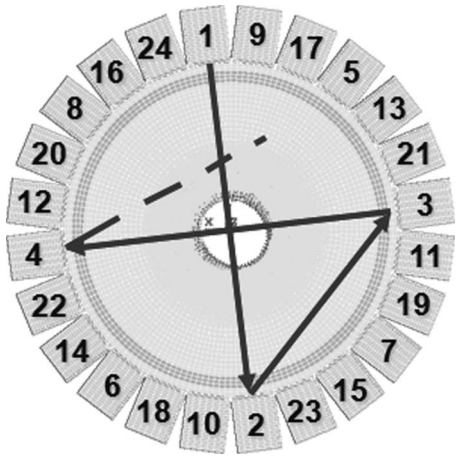

Fig. 7 Geometric pattern with numbers corresponding to the excitation order

The second method to choose the measurement frequencies is a new, improved method, which is used in the maximum test procedure. Distinct from the frequency selection above, the second method chooses the frequencies where the measured blade response is above a given percentage of the maximum response of that blade over the frequency range of interest. This percentage is herein referred to as the response level cut-off. For example, for a response level cut-off of 75% and a maximum response of 150 μm over the frequency range of interest, any frequency with a response magnitude equal to or above 112.5 μm is selected for excitation.

The frequency selection for the maximum test procedure is as follows. After choosing a blade, the system is excited at that blade for all frequencies in a candidate range of frequencies with only the response of that blade being measured. The frequencies with measured responses that are equal to or above the response level cut-off for that blade are selected as excitation frequencies. The other blades are measured for this set of excitation frequencies, and the measurements are used for the mistuning ID. After excitation at a frequency that is applied for any one blade, that frequency is temporarily removed from the list of possible candidate frequencies. Also, all frequencies within a frequency range nearby that applied excitation frequency are removed as well. In this manner, highly localized modes are captured, and little data are duplicated. If the mistuning ID has not converged, the process continues until all the possible frequencies in the range have been excited once. If the mistuning ID still has not met the convergence criteria, then the response level cut-off is lowered, the potential frequency range is increased, and the mistuning ID process is restarted.

Figure 8 contains a sample frequency response. The two horizontal lines show the range of responses considered: from 100% to 75% of the maximum response of that blade. The symbols show the response magnitude at nearby frequencies.

Sample results for the improved frequency selection method using a 75% response level cut-off are shown in Table 2. The initial blade excited is blade 9.

4 Test Procedures

Next, the current sequential test procedure and the (alternate) maximum test procedure are presented. Figure 9 shows the measurement process where the shaded boxes represent the blade and frequency selection processes. Both the maximum and sequential procedures choose an initial excitation blade. After a frequency sweep in the frequency range of interest, the sequential test procedure measures responses at resonances at increasingly higher

Table 2 Blades and frequencies selected using the maximum test procedure

Order tested	Blade No.	Frequency (Hz)
1	9	2144.4
2	21	1981.2; 2068.7; 2105.8
3	15	2127.0
4	3	2072.8; 2164.1
5	12	2118.7

frequencies, while the maximum test procedure chooses frequencies based on a response level cut-off. After those measurements are completed, the maximum test procedure chooses which blade to excite using the geometric pattern, while the sequential chooses the next clockwise blade (as described in Sec. 3.2). Then, the process repeats until the mistuning ID converges or all resonant frequencies for all blades are measured.

5 Test Procedure Validation

A direct comparison between the sequential method and the maximum test procedure can be made by examining the amount of data needed for the mistuning ID convergence and the absolute error obtained for the identified mistuning. Since the initial blade that is excited is arbitrary, multiple trials were conducted to examine the resulting convergence. The trials used every third blade. Trial 1 used blade 1, trial 2 used blade 4, and so on, for a total of eight trials per response level cut-off. One data set was added at a time to the mistuning ID until the 2-norm relative change in the identified mistuning was less than 5% for three consecutive calculations. The 2-norm relative error for the mistuning ID is

$$\text{error} = \frac{\sqrt{\sum_{i=1}^{n} |\mathbf{W}_{i_{\text{previous}}} - \mathbf{W}_{i_{\text{current}}}|^2}}{\sqrt{\sum_{i=1}^{n} |\mathbf{W}_{i_{\text{previous}}}|^2}} \tag{3}$$

where $\mathbf{W}$ is the vector of identified mistuning values, and n is the number of blades. The response level cut-offs used for the maximum test procedure are 0%, 25%, 50%, 75%, and 99%. Note that, for these tests, using a 0% cut-off means that the maximum test procedure and the sequential method are the same, and only one set of data (for one excited blade) is needed to achieve convergence. The 0% case is used as a control since this corresponds to the traditional idea of picking one blade and forcing it at all frequencies before exciting the next blade.

In Fig. 10, the amount of measurement data needed to achieve mistuning ID convergence is displayed on the top. The average of all trials for each response level cut-off is shown on the bottom. All tests were numerically simulated using the 1F family of modes with two measured DOFs per blade. The EIDV procedure was used to determine the best 2 DOF for the frequency range 1900–2180 Hz. The number of measurements is equal to the number of DOFs measured per blade multiplied by the number of blades and the number of measured resonant frequencies. The cost of running a frequency sweep to determine the overall frequency response is ignored.

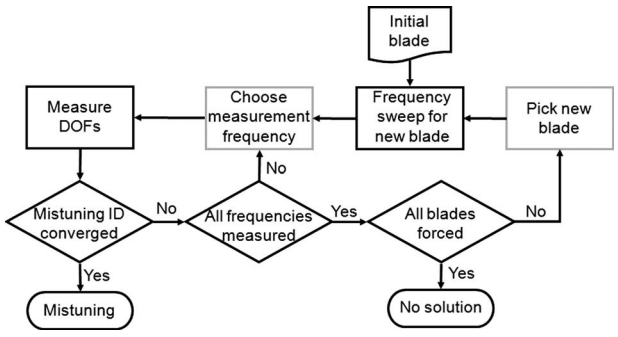

Fig. 9 Test procedure for mistuning ID where the shaded boxes correspond to the blade and frequency selections

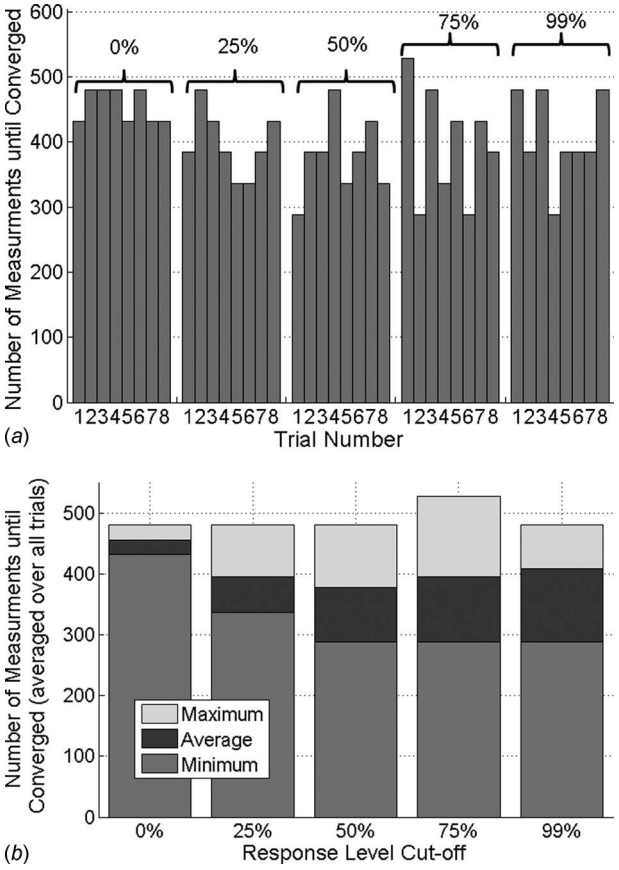

Fig. 10 Number of measurements gathered during mistuning ID using the maximum test procedure

As can be seen in Fig. 10, using a 50%, 75%, or 99% cut-off tends to reduce the amount of measurements needed for mistuning ID. However, the accuracy of the results is more varied, convergence being reached with between 288 and 480 measurements. Figure 10 shows that the average number of measurements using the maximum test procedure is the lowest for a 50% response level cut-off. In general, the maximum test procedure is 11–17% faster than the control results at a response level cut-off of 0%. The maximum amount of time lost using the maximum test procedure is 22% for a 75% response level cut-off. However, the approach may also provide time savings of 40% using either 50%, 75%, or 99% response level cut-off. The most stable response level cut-off is 0% since the variation between the maximum and minimum numbers of measurements required is the lowest. However, this response level cut-off also requires the most number of measurements. In general, the maximum test procedure with the geometric blade selection required less measurements than the control method.

While the average and minimum errors remain consistent for all five tests, the maximum error varies widely. As shown in Fig. 11, the maximum absolute error after convergence decreases as the response level cut-off increases. The improvements vary from 27% to 62%. Therefore, the maximum test procedure with geometric blade choice achieves more accurate and precise results than the 0% response level cut-off case. Note that the maximum normalized absolute error is

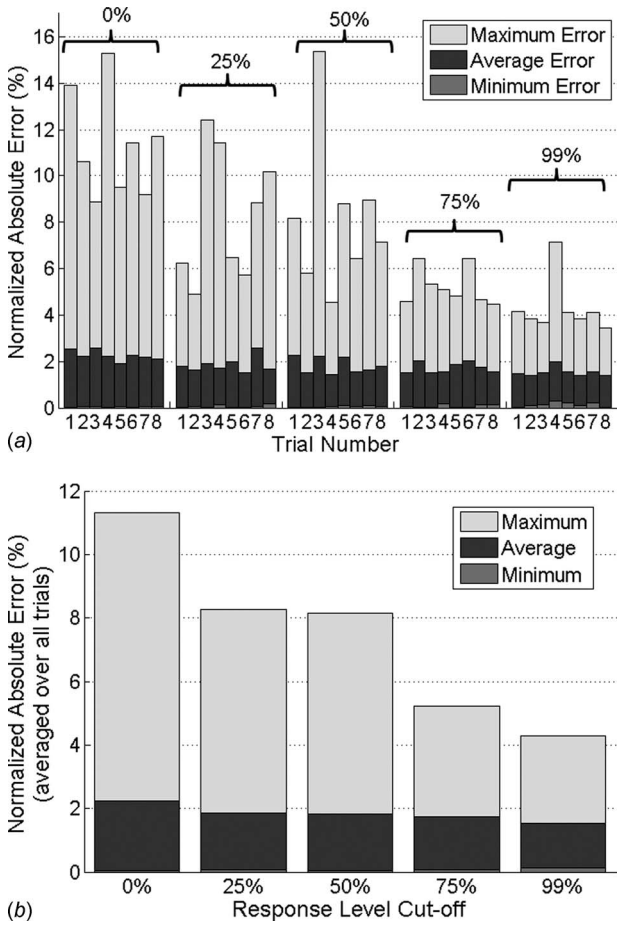

Fig. 11 Normalized absolute error for each trial and response level cut-off after convergence

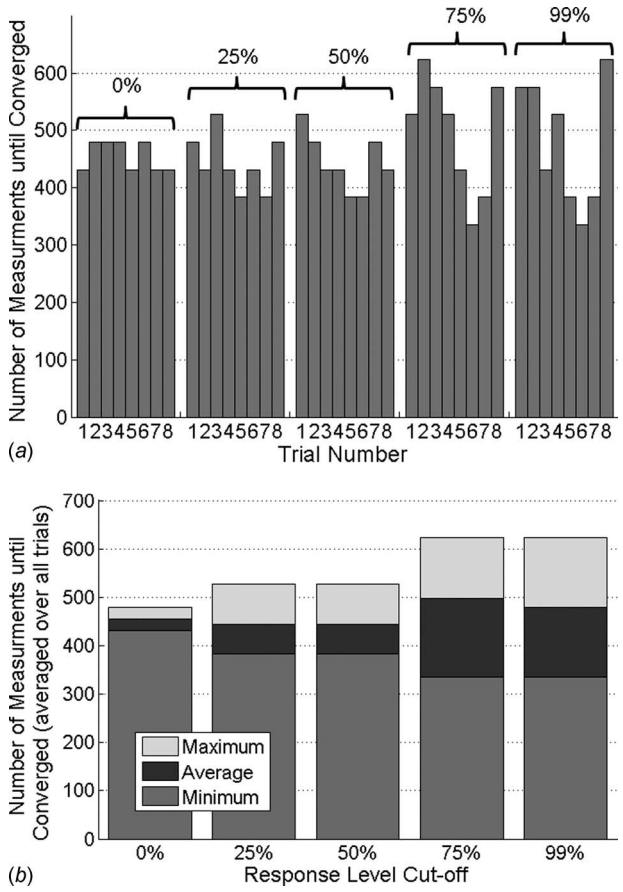

Fig. 13 Number of measurements gathered during mistuning ID using sequential blade selection

$$\text{error}_i = \frac{|\mathbf{W}_{i_{\text{actual}}} - \mathbf{W}_{i_{\text{current}}}|}{\max_i |W_{i_{\text{actual}}}|} \tag{4}$$

where the values have been normalized to the maximum actual blade mistuning value.

Figure 12 shows that the mistuning ID is accurate for determining the mistuning pattern. The minimum, average, and maximum normalized absolute errors for this case are 0.054%, 1.5%, and 4.6%, respectively. A total of 15 modes were used in the ROM for the mistuning ID.

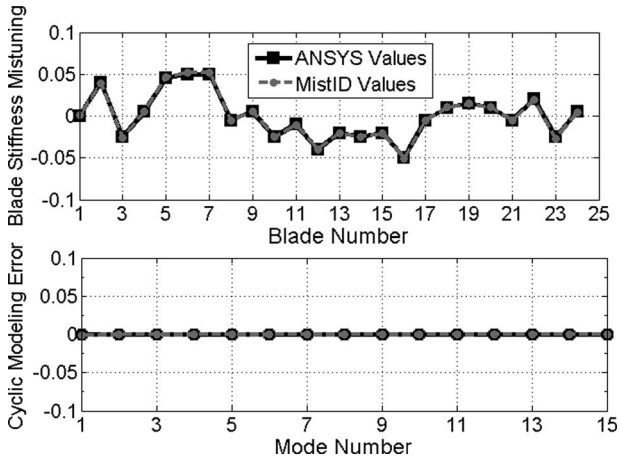

Fig. 12 Mistuning ID results for initial blade 10 and using the maximum test procedure with a 75% response level cut-off

Figure 13 shows a comparison of the results obtained using the maximum test procedure with the sequential blade choice and the control case. These results demonstrate that convergence using the maximum test procedure is not uniform, although the average number of measurements until convergence is approximately the same. The maximum and minimum limits on the number of measurements taken until convergence widen as the response level cut-off increases. Figure 14 shows the same decreasing trend in the maximum normalized absolute error as obtained when using the geometric blade selection, although the improvement is less.

The maximum test procedure with a sequential blade choice provided less uniform convergence with slightly greater accuracy compared with the 0% response level cut-off case with sequential blade selection. The maximum test procedure with a geometric blade selection provided faster convergence with greatly improved accuracy, and is the basis for the maximum test procedure.

6 Calibration

While mistuning ID works without the excitation force being precisely known, faster convergence and greater accuracy can be obtained by calibrating the excitation forcing.

The equation of motion for a blisk can be written as

$$\mathbf{M}\ddot{\mathbf{x}} + (1 + j\gamma)\mathbf{K}\mathbf{x} = \mathbf{f}(t) \tag{5}$$

where γ is the structural damping, and $\mathbf{M}$ and $\mathbf{K}$ are symmetric mass and stiffness matrices.

Considering harmonic motion, $\mathbf{x} = \mathbf{X}e^{i\omega t}$ and $\mathbf{f}(t) = \mathbf{F}e^{i\omega t}$. Denoting $\mathbf{S} = -\omega^2\mathbf{M} + (1 + j\gamma)\mathbf{K}$, Eq. (5) may be rewritten as $\mathbf{X} = \mathbf{S}^{-1}\mathbf{F}$,

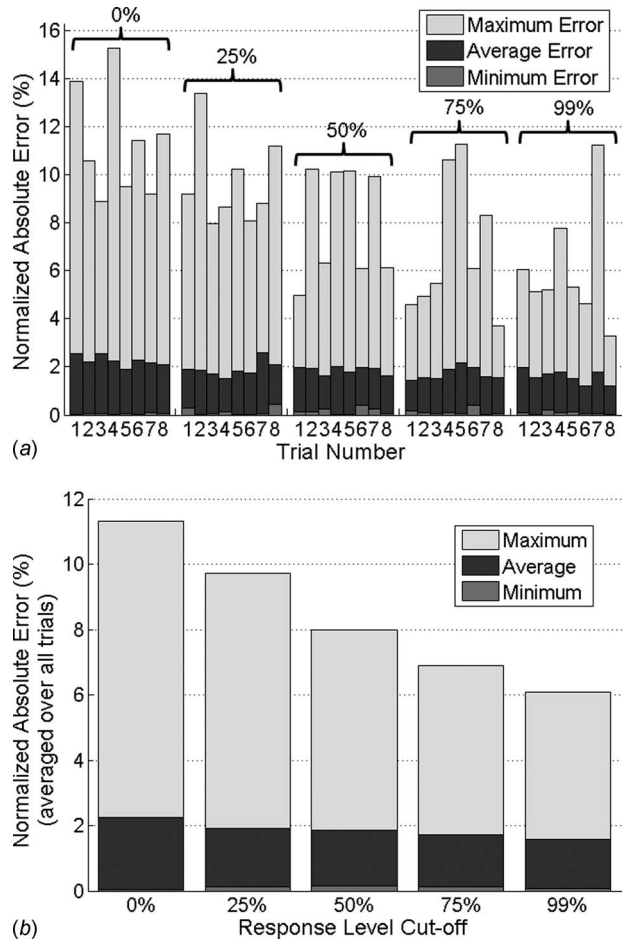

Fig. 14 Normalized absolute error for each trial and response level cut-off after convergence

where $\mathbf{X}$ and $\mathbf{F}$ are matrices built from more than one set of single blade excitation measurement data. Each column in $\mathbf{X}$ is the response obtained for an excitation equal to the corresponding column in $\mathbf{F}$. The flexibility matrix is defined as

$$\mathbf{S}^{-1} = \begin{vmatrix} \alpha_{11} & \alpha_{12} & \cdots & \alpha_{1n} \\ \alpha_{21} & \alpha_{22} & \cdots & \alpha_{2n} \\ \vdots & \vdots & \ddots & \vdots \\ \alpha_{n1} & \alpha_{n2} & \cdots & \alpha_{nn} \end{vmatrix} \tag{6}$$

where α_{lk} is the displacement amplitude at blade l due to a harmonic excitation force with amplitude of 1 at blade k, with all other excitation forces equal to 0, and n is the number of blades.

The matrix $\mathbf{X}$ contains complex response amplitudes and can be written as

$$\mathbf{X} = \begin{vmatrix} X_{11}e^{i\theta_{11}} & X_{12}e^{i\theta_{12}} & \cdots & X_{1n}e^{i\theta_{1n}} \\ X_{21}e^{i\theta_{21}} & X_{22}e^{i\theta_{22}} & \cdots & X_{2n}e^{i\theta_{2n}} \\ \vdots & \vdots & \ddots & \vdots \\ X_{n1}e^{i\theta_{n1}} & X_{n2}e^{i\theta_{n2}} & \cdots & X_{nn}e^{i\theta_{nn}} \end{vmatrix}$$

The response amplitudes have associated magnitudes X_{lk} and phases θ_{lk}, where k and l vary from 1 to n. These response amplitudes correspond to excitation forces of magnitudes F_k and phases Ω_k. The nodal diameter magnitude and phase due to engine-order-excitation are given by $\mathrm{ND}(2\pi/n)$, where ND is the excitation nodal diameter.

If the system is calibrated and noiseless, the phase difference of the response of any two blades exactly matches the phase difference between those two blades for the given engine-order-excitation. Indices l and k are the measured and excited blade numbers, respectively. For single blade excitation measurements involving blades $1-n$ one obtains

$$\mathbf{S}^{-1} \begin{vmatrix} F_1 e^{i\Omega_1} & & & 0 \\ & F_2 e^{i\Omega_2} & & \\ & & \ddots & \\ 0 & & & F_n e^{i\Omega_n} \end{vmatrix} = \mathbf{X} \tag{7}$$

Next, one may define a calibration factor relative to the forcing applied to a reference blade. Choose blade 1 to be the reference blade, so that $F_1 e^{i\Omega_1}$ is the reference excitation force. Denote

$$c_k = \frac{F_k e^{i\Omega_k}}{F_1 e^{i\Omega_1}} \tag{8}$$

Equation (7) becomes

$$F_1 e^{i\Omega_1} \mathbf{S}^{-1} \begin{vmatrix} 1 & & & 0 \\ & c_2 & & \\ & & \ddots & \\ 0 & & & c_n \end{vmatrix} = \mathbf{X} \tag{9}$$

Expanding Eq. (9) into single equations gives $F_1 e^{i\Omega_1} \alpha_{lk} c_k = X_{lk} e^{i\theta_{lk}}$, with $c_1 = 1$.

The principle of reciprocity guarantees that, in a linear system, $\alpha_{kl} = \alpha_{lk}$. Dividing $F_1 e^{i\Omega_1} \alpha_{kl} c_l = X_{kl} e^{i\theta_{kl}}$ by $F_1 e^{i\Omega_1} \alpha_{lk} c_k = X_{lk} e^{i\theta_{lk}}$ and using reciprocity yield

$$\frac{c_l}{c_k} = \frac{X_{kl}}{X_{lk}} e^{i(\theta_{kl} - \theta_{lk})} \quad \text{or} \quad c_l - \frac{X_{kl}}{X_{lk}} e^{i(\theta_{kl} - \theta_{lk})} c_k = 0 \tag{10}$$

Grouping Eq. (10) for all k and l in matrix form and letting $\xi^{kl} = e^{i(\theta_{kl} - \theta_{lk})}$ result in

$$\mathbf{A}\mathbf{c} = \mathbf{b} \tag{11}$$

where

$$\mathbf{A} = \begin{vmatrix} & & \mathbf{I}_{(n,n)} & & \\ -\frac{X_{23}\xi^{23}}{X_{32}} & & & & \\ -\frac{X_{24}\xi^{24}}{X_{42}} & & & & \\ \vdots & & \mathbf{I}_{(n-1,n-1)} & & \\ -\frac{X_{2n}\xi^{2n}}{X_{n2}} & & & & \\ 0 & -\frac{X_{34}\xi^{34}}{X_{43}} & & & \\ 0 & -\frac{X_{35}\xi^{35}}{X_{53}} & & & \\ \vdots & \vdots & & \mathbf{I}_{(n-2,n-2)} & \\ 0 & -\frac{X_{3n}\xi^{3n}}{X_{n3}} & & & \\ & \ddots & & \ddots & \\ 0 & \cdots & 0 & -\frac{X_{(n-1)n}\xi^{(n-1)n}}{X_{n(n-1)}} & 1 \end{vmatrix}$$

$$\mathbf{c} = \begin{Bmatrix} c_2 \\ c_3 \\ \vdots \\ c_n \end{Bmatrix} \quad \text{and} \quad \mathbf{b} = \begin{Bmatrix} \frac{X_{12}\xi^{12}}{X_{21}} \\ \frac{X_{13}\xi^{13}}{X_{31}} \\ \vdots \\ \frac{X_{1n}\xi^{1n}}{X_{n1}} \\ 0 \\ \vdots \\ 0 \end{Bmatrix}$$

The calibration is now posed as a least-squares problem where Eq. (11) is solved for $\mathbf{c}$, with c_2 to c_N being the linear calibration factors.

The calibration process involves exciting blade k and measuring blade l for all blades on the blisk. Data from exciting and measuring the same blade are ignored since these result in $c_k - c_k = 0$. Once the least-squares problem is solved, the new excitation magnitude from Eq. (8) becomes $F_k = |c_k| F_1$. Assuming a linear relationship, $F_{k_{\text{new}}} = F_k / |c_k|$. Likewise, the new phases are obtained by finding the principle log of $\arg(c_k)$, resulting in

$$\Omega_k = \phi_k + \Omega_1 \tag{12}$$

where ϕ_k is the calibration phase. The calibration phase represents the actual excitation phase with respect to the reference blade. Denoting Ω_k as $\Omega_k = \Phi_k + \Delta\Phi_k$, where Φ_k is the engine-order-excitation phase, and $\Delta\Phi_k$ is the phase error for the excitation at blade k, Eq. (12) becomes

$$\Phi_k + \Delta\Phi_k = \phi_k + \Phi_1 + \Delta\Phi_1 \tag{13}$$

Since blade 1 was used as a reference, $\Phi_1 = 0$ and $\Delta\Phi_1 = 0$, so $\Delta\Phi_k = \phi_k - \Phi_k$. Assuming a linear relationship, the new phase of the excitation becomes

$$P_{\text{new}} = P_{\text{old}} - \Delta\Phi_k = P_{\text{old}} + \Phi_k - \phi_k \tag{14}$$

where P_{new} is the new excitation phase, and P_{old} is the excitation phase for blade k during calibration measurements. For example, if the excitation phase before calibration is 28 deg, the desired engine-order-excitation phase referenced to blade 1 is 30 deg, and the phase calibration angle is 31 deg, then $P_{\text{new}} = 28$ deg $+30$ deg -31 deg $=27$ deg.

Perfect calibration occurs when $F_2, F_3, \ldots, F_4 = F_1$, or $|c_2|, |c_3|, \ldots, |c_N| = 1$ and $\arg(c_2) = e^{i\Theta_2}$, $\arg(c_2) = e^{i\Theta_3}, \ldots,$ $\arg(c_N) = e^{i\Theta_N}$, where Θ_k is the phase of the engine-order-excitation corresponding to blade k with reference to blade 1.

For calibrating single blade excitation, only the amplitude needs to be considered. However, engine-order-excitation (which simulates the forcing that a blisk will receive in an engine) requires calibration of both the amplitude and phase. Since nonlinear factors (such as variation in the excitation force with the distance to the excited blade) occur, iterations using the new calibration factors should be completed until coefficients c_2 to c_N are within a desired error level.

Note that the calibration depends on displacements, but measurements using a laser vibrometer are typically velocities. Since the blisk is (very lightly and) structurally damped and it undergoes harmonic motion, the displacements are proportional to the velocities, and may be replaced with scaled velocities. However, this is unnecessary because the scaling of the velocities cancels out in Eq. (10) where only the ratios X_{kl}/X_{lk} are needed.

Testing the calibration procedure produced excellent results within a few iterations. In Fig. 15, the magnitudes of the calibration factors have maximum and average values of 3.9 and 1.8, respectively. At the end of two iterations, the maximum value is 1.01 and the average value is 0.99. The phase corrections, also shown in Fig. 15, start with a maximum value of 9.0 deg, and end with a maximum value of 0.52 deg. The average phase errors decrease from 4.0 deg to 0.24 deg.

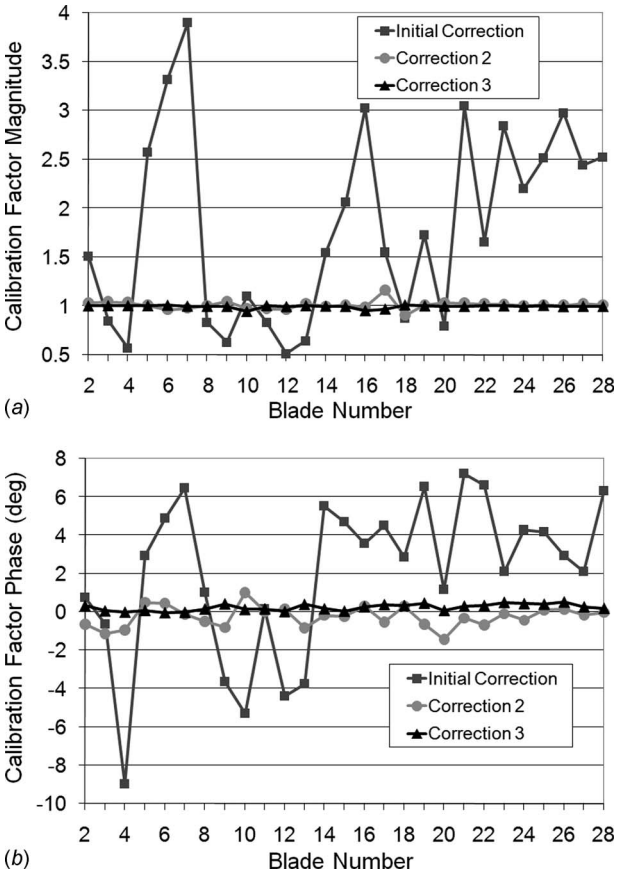

Fig. 15 Experimental results from three iterations of the calibration procedure for an engine-order-excitation 0

In addition, failure to calibrate can indicate a hardware problem. During the testing, one of the magnets was connected to a loose electronic chip. That defect was detected through the calibration process. When fixed, all magnets were calibrated to within 0.5% of blade 1 forcing. Also, a sensitivity analysis showed that a 1% error in measurements resulted in a 1% error in calibration.

Because the calibration works for both magnitude and phase, the results indicate how much actuation and accuracy the excitation system can produce. The first calibration can be performed using an engine-order-excitation 0 for which all blades are in phase. This provides a baseline for further testing and calibration. Note that calibration may be carried out at frequencies characterized by a mistuned response. However, the signal to noise ratio will be higher than that at frequencies where the response is closer to the tuned response, resulting in a less accurate calibration.

7 Conclusion and Discussion

In this work, an integrated testing and calibration procedure was presented for performing mistuning ID and TWE of blisks. This procedure yields accurate results, is highly efficient, and is characterized by three key features.

First, a novel measurement point selection method was presented. In this method, a truncated set of modes from a finite element model of a tuned blisk is used in a modified EIDV method. This enables one to determine a minimal set of measurement DOF (and locations) that works well for mistuning ID. The EIDV procedure attempts to maximize linear independence of the measured (physical) DOF, resulting in more accurate physical to

modal transformations for the test data. Also the automatic nature of EIDV provides an efficient method for selecting measurement DOF (and locations).

Second, a new testing procedure was presented that allows the mistuning to be identified from relatively few vibration response measurements. Numerical experiments were used to investigate the convergence of the mistuning ID approach for a prescribed mistuning pattern using the proposed approach and alternative testing strategies. Using the proposed method, the total number of measurements and corresponding time savings decrease from 11% to 22% along with a decrease in the maximum normalized absolute error of 27–62%.

Although the EIDV and test procedures were numerically validated, an experimental validation is also desirable. In this paper, the effects of measurement noise and uncertainties were ignored in order to provide perspective on the benefits of the proposed test procedure separated from other issues such as signal processing, data filtering, etc., which are part of the experimental work. In general, it is expected that measurement noise will likely lengthen the time required to achieve convergence in the mistuning ID. Since the sequential method includes measurements with low amplitudes, that method is more susceptible to errors due to noise than the maximum test procedure (which contains data with larger amplitudes).

Third, a novel method was derived to iteratively calibrate the forcing applied to each blade of a blisk so that differences among the blade forcing magnitudes can be minimized for single blade excitation. Also, the calibration ensures that the phases of the excitations applied to each of the blades can be accurately set for TWE. The calibration increases the mistuning ID accuracy by eliminating force mistuning. The calibration algorithm uses the principle of reciprocity and involves solving a least-squares problem to reduce the effects of measurement noise and uncertainty. Experimental validation of the calibration method and TWE calibration on a blisk with relatively complex geometry were completed.

Acknowledgment

This work was supported by GE Aviation through the University Strategic Alliance (USA) program, with George Sandusky as the program manager, Darin DiTommaso as the section manager, and Steve Manwaring as the subsection manager. The authors would also like to thank Frank Gardner of GE Aviation and Tommy George of the Air Force Research Laboratory for their help in setting up and running the experiments.

Nomenclature

blisk(s) = bladed disk(s)

References

[1] Srinivasan, A. V., 1997, "Flutter and Resonant Vibration Characteristics of Engine Blades," ASME J. Eng. Gas Turbines Power, **119**(4), pp. 742–775.
[2] Slater, J. C., Minkiewicz, G. R., and Blair, A. J., 1999, "Forced Response of Bladed Disk Assemblies—A Survey," Shock Vib. Dig., **31**(1), pp. 17–24.
[3] Castanier, M. P., and Pierre, C., 2006, "Modeling and Analysis of Mistuned Bladed Disk Vibration: Status and Emerging Directions," J. Propul. Power, **22**(2), pp. 384–396.
[4] Thomson, D. E., and Griffin, J. T., 1999, "The National Turbine Engine High Cycle Fatigue Program," The Global Gas Turbine Newsletter (GGTN), **39**(1), pp. 14–17.
[5] Judge, J., Pierre, C., and Ceccio, S. L., 2001, "Experimental Identification of Mistuning in Blisks," *Proceedings of the 6th National Turbine Engine High Cycle Fatigue Conference*, Universal Technology Corporation, Dayton, OH.
[6] Judge, J., Pierre, C., and Ceccio, S. L., 2001, "Experimental Validation of Mistuning Identification Techniques and Vibration Predictions in Bladed Disks," *Proceedings of the International Forum on Aeroelasticity and Structural Dynamics*, Madrid, Spain.
[7] Mignolet, M., Rivas-Guerra, A., and Delor, J., 2001, "Identification of Mistuning Characteristics of Bladed Disks From Free Response Data—Part I," ASME J. Eng. Gas Turbines Power, **123**(2), pp. 395–403.
[8] Rivas-Guerra, A., Mignolet, M., and Delor, J., 2001, "Identification of Mistuning Characteristics of Bladed Disks From Free Response Data—Part II," ASME J. Eng. Gas Turbines Power, **123**(2), pp. 404–411.
[9] Pichot, F., Thouverez, F., Jezequel, L., and Seinturier, E., 2001, "Mistuning Parameters Identification of a Bladed Disk," Key Eng. Mater., **204–205**, pp. 123–132, URL: http://www.scientific.net.
[10] Judge, J., Pierre, C., and Mehmed, O., 2001, "Experimental Investigation of Mode Localization and Forced Response Amplitude Magnification for a Mistuned Bladed Disk," ASME J. Eng. Gas Turbines Power, **123**(4), pp. 940–950.
[11] Judge, J. A., Pierre, C., and Ceccio, S. L., 2002, "Mistuning Identification in Bladed Disks," *Proceedings of the International Conference on Structural Dynamics Modelling*, Madeira, Portugal.
[12] Pierre, C., Judge, J., Ceccio, S. L., and Castanier, M. P., 2002, "Experimental Investigation of the Effects of Random and Intentional Mistuning on the Vibration of Bladed Disks," *Proceedings of the 7th National Turbine Engine High Cycle Fatigue Conference*, Universal Technology Corporation, Dayton, OH.
[13] Feiner, D. M., and Griffin, J., 2003, "A Completely Experimental Method of Mistuning Identification in Integrally Bladed Rotors," *Proceedings of the 8th National Turbine Engine High Cycle Fatigue Conference*, Universal Technology Corporation, Dayton, OH, pp. 1.1–1.13.
[14] Kim, N. E., and Griffin, J., 2003, "System Identification in Higher Modal Density Regions of Bladed Disks," *Proceedings of the 8th National Turbine Engine High Cycle Fatigue Conference*, Universal Technology Corporation, Dayton, OH, pp. 1.68–1.82.
[15] Feiner, D., and Griffin, J., 2004, "Mistuning Identification of Bladed Disks Using a Fundamental Mistuning Model—Part I: Theory," ASME J. Turbomach., **126**(1), pp. 150–158.
[16] Feiner, D., and Griffin, J., 2004, "Mistuning Identification of Bladed Disks Using a Fundamental Mistuning Model—Part II: Application," ASME J. Turbomach., **126**(1), pp. 159–165.
[17] Lim, S.-H., Castanier, M. P., and Pierre, C., 2004, "Mistuning Identification and Reduced-Order Model Updating for Bladed Disks Based on a Component Mode Mistuning Technique," *Proceedings of the 9th National Turbine Engine High Cycle Fatigue Conference*, Universal Technology Corporation, Dayton, OH.
[18] Lim, S.-H., Pierre, C., and Castanier, M. P., 2006, "Predicting Blade Stress Levels Directly From Reduced-Order Vibration Models of Mistuned Bladed Disks," ASME J. Turbomach., **128**(1), pp. 206–210, URL: http://dx.doi.org/10.1115/1.2098754.
[19] Lim, S., Bladh, R., Castanier, M. P., and Pierre, C., 2007, "Compact, Generalized Component Mode Mistuning Representation for Modeling Bladed Disk Vibration," AIAA J., **45**(9), pp. 2285–2298.
[20] Li, J., Pierre, C., and Ceccio, S. L., 2005, "Validation of a New Technique for Mistuning Identification and Model Updating Based on Experimental Results for an Advanced Bladed Disk Prototype," *Evaluation, Control and Prevention of High Cycle Fatigue in Gas Turbine Engines for Land, Sea and Air Vehicles (Meeting Proceedings RTO-MP-AVT-121)*, NATO Research and Technology Organisation, Neuilly-sur-Seine, France, pp. 36.1–36.16.
[21] Pichot, F., Laxalde, D., Sinou, J. J., Thouverez, F., and Lombard, J. P., 2006, "Mistuning Identification for Industrial Blisks Based on the Best Achievable Eigenvector," Comput. Struct., **84**(29–30), pp. 2033–2049.
[22] Laxalde, D., Thouverez, F., Sinou, J.-J., Lombard, J.-P., and Baumhauer, S., 2007, "Mistuning Identification and Model Updating of an Industrial Blisk," Int. J. Rotating Mach., **2007**(17289), pp. 1–10, URL: http://dx.doi.org/10.1155/2007/17289.
[23] Li, J., 2007, "Experimental Investigation of Mistuned Bladed Disks System Vibration," Ph.D. thesis, University of Michigan, Ann Arbor, MI.
[24] Madden, A. C., Castanier, M. P., and Epureanu, B. I., 2008, "Reduced-Order Model Construction Procedure for Robust Mistuning Identification of Blisks," AIAA J., **46**(11), pp. 2890–2898.
[25] Judge, J. A., 2002, "Experimental Investigations of the Effects of Mistuning on Bladed Disk Dynamics," Ph.D. thesis, University of Michigan, Ann Arbor, MI.
[26] Penny, J. E. T., Friswell, M. I., and Garvey, S. D., 1994, "Automatic Choice of Measurement Locations for Dynamic Testing," AIAA J., **32**(2), pp. 407–414.
[27] Kammer, D. C., 1991, "Sensor Placement for On-Orbit Modal Identification and Correlation of Large Space Structures," J. Guid. Control Dyn., **14**(2), pp. 251–259.